applied sciences

MDPI

Article

Analysis of Dynamic Characteristics for Robust Control of the Single Suspension Electromagnet System on a Flexible Beam

Keren Wang [1,2], Junxiong Hu [3,4], Weihua Ma [5] and Xiaohao Chen [6,7,*]

[1] Department of Intelligent Manufacturing, Leshan Vocational and Technical College, Leshan 614000, China; muhuaren183@126.com
[2] School of Computing and Artificial lntelligence, Southwest Jiaotong University, Chengdu 611756, China
[3] Maglev Transportation Engineering R&D Center, Tongji University, Shanghai 201804, China; hujx92@outlook.com
[4] State Key Laboratory of High-Speed Maglev Transportation Technology, Qingdao 266111, China
[5] State Key Laboratory of Traction Power, Southwest Jiaotong University, Chengdu 610031, China; mwh@swjtu.cn
[6] Key Laboratory of Intelligent Operation and Maintenance Technology and Equipment for Urban Track Transit of Zhejiang Province, Zhejiang Normal University, Jinhua 321004, China
[7] College of Engineering, Zhejiang Normal University, Jinhua 321004, China
* Correspondence: xiaohao_chen@zjnu.edu.cn

Abstract

To minimize the construction cost of track beam and enhance the dynamic performance of the magnetic suspension system, a simplified coupled vibration model of the electromagnet-track beam-vehicle body was established. Initially, by defining a Lyapunov function to represent the quadratic performance index of the maglev system under parameter perturbation, the controller design problem for the closed-loop system was transformed into an existence problem of linear matrix inequality (LMI) solutions. Consequently, a state-feedback cost-preserving robust controller for a flexible track beam was designed. Subsequently, the impact of the suspension controller on the dynamic characteristics of the flexible track beam, both with and without considering parameter perturbation, was compared and analyzed. Furthermore, the robustness, high-frequency suppression, and low-frequency following characteristics of the LMI-based controller were evaluated. Finally, the influence of two distinct state feedback controllers on the dynamic characteristics of the flexible track beam across different frequency bands was analyzed. Correlation analysis revealed that accounting for parameter perturbation can improve the suspension and dynamic characteristics of the suspension controller. When the system experiences parameter perturbation, the LMI-based suspension controller can achieve stable suspension on the flexible track beam while demonstrating strong robustness, high-frequency suppression, and low-frequency following capabilities. On the flexible beam, controllers with different state feedback exhibit varying dynamic characteristics in different vibration frequency segments of the track beam. Specifically, reducing the feedback state variables in the low-frequency band and increasing them in the high-frequency band can appropriately improve the system's dynamic characteristics.

Keywords: magnetic suspension system; coupling vibration; flexible track beam; parameter perturbation; state-feedback cost-preserving robust controller

Check for updates

Received: 2 February 2026
Revised: 5 March 2026
Accepted: 6 March 2026
Published: 8 March 2026

Copyright: © 2026 by the authors. Licensee MDPI, Basel, Switzerland. This article is an open access article distributed under the terms and conditions of the Creative Commons Attribution (CC BY) license.

1. Introduction

The maglev train, characterized by high speed, low noise, and energy efficiency, has emerged as a pivotal mode of modern transit [1–6]. While commercial operations using Electromagnetic Suspension (EMS) technology have expanded globally—including lines in South Korea and various Chinese cities—the inherent instability of EMS systems remains a critical challenge. EMS relies on active control to maintain a narrow suspension gap (typically 8–10 mm) against the nonlinear inverse relationship between electromagnetic force and gap distance. This complex interaction creates a multidisciplinary, coupled system comprising the vehicle, suspension control, and elastic track beam. Consequently, coupling vibrations between the vehicle and the track are frequently observed, posing significant risks to operational safety and system stability [2,7].

Extensive research has been devoted to understanding and mitigating these coupling vibrations, primarily falling into three categories: dynamic system modeling, suspension frame optimization, and controller design.

Regarding dynamic characteristics and modeling, scholars have established that the flexibility of the track beam significantly influences system stability. Early studies utilized Bernoulli-Euler beam models to analyze vehicle–track interactions at varying speeds and explore the dynamic characteristics of the maglev vehicle–track beam coupling system [8,9]. Subsequent research incorporated flexible support structures and three-dimensional coupling models, confirming that track irregularities and structural flexibility are primary excitations for self-excited vibrations [10–13]. Crucially, Li et al. identified the suspension control system itself as the primary energy source for these self-excited vibrations, while others analyzed stability boundaries using Hopf bifurcation theory [14–22]. Although these studies provide a comprehensive theoretical foundation for understanding vibration mechanisms, they largely focus on describing the phenomenon rather than offering cost-effective mitigation strategies for engineering applications.

To address vibration issues, some researchers have proposed optimizing the mechanical running mechanism. Innovations such as new suspension frames and mid-mounted single-suspension designs with air springs have demonstrated improved ride comfort and dynamic performance in simulations and experiments [23,24]. However, while effective, modifying the mechanical structure often entails significant redesign costs and may not be feasible for existing infrastructure.

Consequently, the majority of recent efforts have focused on suspension controller design to suppress vibrations without altering hardware. Approaches include optimizing PID parameters, introducing virtual tuned mass dampers (VTMD), and employing advanced strategies like adaptive sliding mode control and neural network-based algorithms [25–32]. These methods have successfully enhanced disturbance rejection and stability under ideal conditions. In practice, however, maglev systems face inevitable parameter perturbations due to environmental changes, component aging, magnetic saturation, and varying passenger loads. While some studies have attempted to address robustness using Linear Quadratic (LQ) optimal control or variable boundary layer sliding mode control [33–35], these methods often fail due to insufficient adaptability to complex nonlinearities. Furthermore, deep learning and neural network approaches, while promising, often require extensive training data and lack the interpretability required for safety-critical certification [36,37]. Although the above-mentioned literature has achieved satisfactory control results, there is a lack of research quantifying how advanced state-feedback strategies can allow for the use of lower-stiffness flexible track beams while suppressing coupling vibrations. Furthermore, the optimal selection of state feedback variables based on specific vibration frequency ranges remains unexplored.

A fundamental economic constraint further complicates this issue. Current engineering practices often mitigate coupling vibrations by increasing the mass and stiffness of the track beam. However, track beam construction accounts for a substantial proportion of total maglev line costs [38]. Therefore, relying on heavier infrastructure to ensure stability is economically inefficient. There is an urgent need for control strategies that can guarantee stable levitation on lighter, more flexible track beams, even in the presence of significant parameter perturbations.

While recent work has begun to incorporate track vibration states into feedback loops [39–42], a significant gap remains: existing multi-state feedback controllers generally assume precise system models and fail to simultaneously address the dual challenges of track flexibility and parametric uncertainty. Specifically, prior designs do not adequately account for how parameter perturbations degrade the stability margins of controllers tuned for flexible beams, leading to potential resonance or instability when real-world deviations occur.

To bridge this gap, this paper proposes a robust suspension control strategy based on Linear Matrix Inequality (LMI) formulation. Unlike conventional methods that prioritize nominal performance, our approach explicitly integrates parameter perturbation bounds directly into the controller synthesis phase while simultaneously accounting for the flexible vibration states of both the track beam, the electromagnet and the vehicle body. By defining a Lyapunov function to represent the system's quadratic performance index, we transform the robust controller design problem into a convex optimization problem solvable via LMI techniques. This method offers two distinct advantages:

1. Guaranteed Robustness: It mathematically ensures closed-loop stability and performance constraints even when system parameters deviate from their nominal values.
2. Flexibility Compatibility: It enables the active suppression of coupling vibrations on lightweight, flexible track beams, thereby reducing the reliance on costly, heavy infrastructure.

This study demonstrates that the proposed LMI-based controller not only maintains stable suspension under parameter perturbations but also optimizes the energy flow between the vehicle and the flexible track, offering a viable pathway to reduce maglev system construction costs without compromising safety or ride comfort.

The structure of this paper is as follows:

- Step 1 formulates the dynamic model and derives the state-space equations for the maglev system.
- Step 2 details the design methodology for the proposed robust controller, specifically addressing parametric perturbations through Linear Matrix Inequality (LMI) techniques.
- Step 3 defines two distinct control strategies for comparative analysis, building upon the framework in [42]:
  - Controller 1: A conventional state feedback controller that actively regulates only the suspension electromagnet.
  - Controller 2: An advanced multi-variable state feedback controller that simultaneously manages the vibration states of the electromagnet, the elastic track beam, and the car body.
- Step 4 evaluates the impact of these controllers on system stability. By analyzing the maximum eigenvalues of the closed-loop system under varying track beam stiffness, we compare the stability margins of Controller 1 and Controller 2. Furthermore, using the elastic track beam as a case study, this section assesses the performance of Controller 2 under both nominal conditions and in the presence of parametric

perturbations, with a specific focus on the energy work done by the suspension system on the track.

- Step 5 provides a comprehensive robustness analysis of the LMI-based controller, verifying its ability to maintain stable levitation despite significant system parameter variations.
- Step 6 presents a theoretical analysis of energy flow characteristics across the different state feedback methods applied to the flexible beam, linking control strategies to dynamic performance.
- Step 7 summarizes the key findings and concludes the study.
- Step 8 summary of research shortcomings and outlook.

2. Vertical Coupled Vibration Model

2.1. Equivalent Model of Coupling Vibration Vehicle-Guideway

By employing the decoupling method, the maglev system can be simplified into a single magnet control problem. Ensuring the stability of an individual magnet is crucial for maintaining the stable operation of the maglev train. Consequently, a coupled vibration model of the single magnetic-elastic track beam-car body is developed (as illustrated in Figure 1).

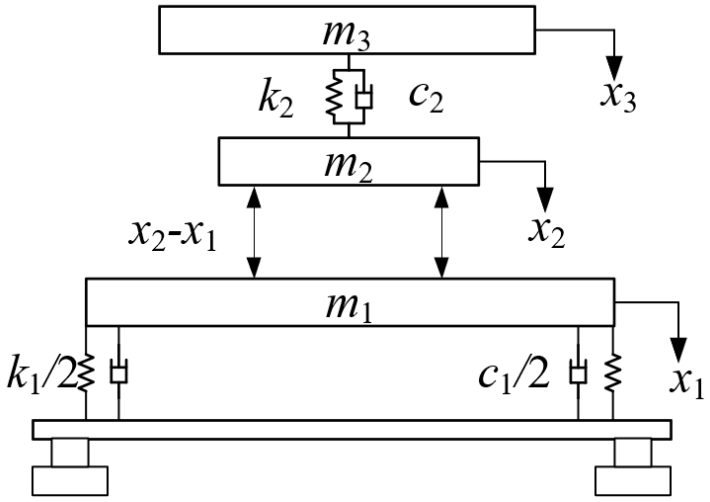


Figure 1. Maglev vehicle vehicle-guideway model.

In this model, m_1 denotes the equivalent mass of the track beam, while m_2 and m_3 represent the masses of the suspension electromagnet and the body, respectively. k_1 and c_1 signify the equivalent stiffness and damping coefficient of the support beam, respectively. k_2 and c_2 correspond to the stiffness and damping coefficient of the secondary suspension system. x_1, x_2, and x_3 indicate the displacements of the support beam, the electromagnet, and the vehicle body relative to their nominal positions, respectively.

When the suspension electromagnet is energized, the instantaneous suspending force F_m generated by the electromagnet can be derived using Maxwell's Equations:

$$F_m = \frac{B_m}{\mu} A_m \tag{1}$$

The electromagnetic strength B_m is defined as follows:

$$B_m = \frac{\mu n i}{2c} \tag{2}$$

By substituting Equation (2) into Equation (1), the electromagnetic force Equation for a suspended electromagnet can be expressed as follows:

$$F_m(i,c) = \frac{\mu n^2 A_m}{4}\left(\frac{i}{c}\right)^2 \tag{3}$$

The magnetic flux linkage ψ of the electromagnet coil can be derived from magnetic circuit analysis:

$$\psi = n\varphi = \frac{\mu A_m n^2}{2c} i \tag{4}$$

The inductance L of the electromagnet is therefore a function of the air gap c:

$$L(c) = \frac{\psi}{i} = \frac{\mu A_m n^2}{2c} \tag{5}$$

The voltage Um across the coil terminals is given by Faraday's law and Kirchhoff's voltage law:

$$U_m = iR + \frac{d\psi}{dt} = iR + \frac{d}{dt}[L(c)i] \tag{6}$$

Expanding the derivative using the chain rule, and noting that L is a function of c which varies with time:

$$U_m = iR + \frac{di}{dt}L(c) + i\frac{dL}{dc}\frac{dc}{dt}$$

Since $\frac{dL}{dc} = -\frac{\mu A_m n^2}{2c^2} = -\frac{L(c)}{c}$, it can be obtained as follows:

$$U_m = iR + \frac{di}{dt}L(c) - i\frac{L(c)}{c}\frac{dc}{dt} \tag{7}$$

The Taylor expansion of Equation (7) is performed at the rated operating point (i_0,c_0,U_0):

Let $i = i_0 + \Delta i$, $c = c_0 + \Delta c$, $U_m = U_0 + \Delta U$. At the equilibrium point, $\frac{di}{dt} = 0$ and $\frac{dc}{dt} = 0$, so $U_0 = i_0 R$. Expanding each term:

$iR \approx i_0 R + R\Delta i$, $L(c) \approx L(c) + \left.\frac{dL}{dc}\right|_0 \Delta c = L_0 - \frac{L_0}{c_0}\Delta c$, where $L_0 = \frac{\mu A_m n^2}{2c_0}$. Therefore, $L(c)\frac{di}{dt} \approx L_0\frac{d(\Delta i)}{dt}$, neglecting the second-order term $-\frac{L_0}{c_0}\Delta c\frac{d(\Delta i)}{dt}$. For the last term, $-\frac{L(c)}{c}i\frac{dc}{dt}$, the coefficient at the operating point is $-\frac{L_0}{c_0}i_0$. Keeping the first-order term gives $-\frac{i_0 L_0}{c_0}\frac{d(\Delta c)}{dt}$. Substituting and subtracting the steady-state equation $U_0 = i_0 R$:

$$\Delta U = \Delta i R + L_0\Delta\dot{i} - L_0\frac{i_0}{c_0}\Delta\dot{c} \tag{8}$$

To simplify the control equations, we define force sensitivity parameters P_s and P_i based on Equation (3):

Current Stiffness: $P_i = \left.\frac{\partial F_m}{\partial i}\right|_0 = \frac{\mu n^2 A_m}{4}\frac{2i_0}{c_0^2} = \frac{\mu n^2 A_m}{2c_0^2} i_0$.

Gap Stiffness Factor: $P_s = \left.\frac{\partial F_m}{\partial c}\right|_0 = \frac{\mu n^2 A_m}{2c_0^3} i_0^2$.

$$\frac{P_s}{P_i} = \frac{i_0}{c_0} \tag{9}$$

Based on Equations (8) and (9), the electrical Equation of the suspension system at the equilibrium position can be expressed as follows [40]:

$$\Delta\dot{i} = -\frac{R}{L_0}\Delta i + \frac{i_0}{c_0}\Delta\dot{c} + \frac{\Delta U}{L} \tag{10}$$

After expanding and applying Taylor's theorem to Equation (3) at the equilibrium position, we obtain the dynamic equation describing the fluctuation of the suspended electromagnetic levitation force around this stable point as follows [40]:

$$\Delta F = P_i \Delta i - P_s \Delta c \tag{11}$$

In Equations (1) to (11), U_m represents the voltage actually applied across the suspended electromagnet coil, φ denotes the magnetic flux through the pole area of the suspended electromagnet, L_m is the instantaneous inductance of the electromagnet, c is the actual suspension gap, and U_0 is the voltage across the electromagnet coil at the equilibrium position. P_s and P_i represent the air gap coefficient and current coefficient, respectively, at the equilibrium position of the suspended electromagnet. μ is the vacuum permeability, n is the number of coil turns, i is the instantaneous current flowing through the suspended electromagnet, i_0 is the current at the equilibrium position, Δi is the change in current relative to the equilibrium position, c_0 is the suspension gap at the equilibrium position, A_m is the pole area of the suspended electromagnet, and Δc is the change in air gap relative to the equilibrium position. Note: All the formula derivations above are based on the following assumptions: The system undergoes only small vibrations in the vicinity of the equilibrium position. Consequently, higher-order terms are neglected; The ferromagnetic core material operates within its unsaturated region, the permeability μ is therefore considered constant, and hysteresis effects are absent; The magnetic field within the air gap is assumed to be uniform, with flux lines perpendicular to the pole faces. Leakage flux is disregarded.

Considering the model illustrated in Figure 1 as the research object, the dynamic equations for the track beam, suspended electromagnet, and car body at the rated suspension position can be derived based on Newton's second law. These equations are presented as Equation (12), Equation (13) and Equation (14), respectively.

$$m_1 \ddot{x}_1 = \Delta F - k_1 x_1 - c_1 \dot{x}_1 \tag{12}$$

$$m_2 \ddot{x}_2 = -\Delta F + (x_3 - x_2) k_2 + (\dot{x}_3 - \dot{x}_2) c_2 \tag{13}$$

$$m_3 \ddot{x}_3 = -(x_3 - x_2) k_2 - (\dot{x}_3 - \dot{x}_2) c_2 \tag{14}$$

Combining Equations (11) and (12) results in:

$$\ddot{x}_1 = \frac{P_i}{m_1} \Delta i - \frac{P_s}{m_1} \Delta c - \frac{k_1}{m_1} x_1 - \frac{c_1}{m_1} \dot{x}_1 \tag{15}$$

Combining Equation (11) and Equation (13) results in:

$$\ddot{x}_2 = \frac{P_s}{m_2} \Delta c - \frac{P_i}{m_2} \Delta i + \frac{k_2}{m_2} (x_3 - x_2) + \frac{c_2}{m_2} (\dot{x}_3 - \dot{x}_2) \tag{16}$$

By differentiating both sides of Equation (16), we derive the following result:

$$\dddot{x}_2 = \frac{P_s}{m_2} \Delta \dot{c} - \frac{P_i}{m_2} \Delta \dot{i} + \frac{k_2}{m_2} (\dot{x}_3 - \dot{x}_2) + \frac{c_2}{m_2} (\ddot{x}_3 - \ddot{x}_2) \tag{17}$$

By integrating Equation (1) through Equation (17), and considering x_1, $\dot{x}_1$, x_2, $\dot{x}_2$, $\ddot{x}_2$, x_3, $\dot{x}_3$ as the state variable, that is, in Equation (18), X is $[x_1 \dot{x}_1 x_2 \dot{x}_2 \ddot{x}_2 x_3 \dot{x}_3]$. At the same time, levitation gap and electromagnet acceleration will be used as outputs, that is, in Equation (18), Y is $[x_2 - x_1, \ddot{x}_2]^{\mathrm{T}}$. The state-space representation of the coupled

vibration model for the car body-suspended electromagnet-elastic track beam system can be derived as follows:

$$\begin{cases} \dot{X} = AX + Bu \\ Y = CX \end{cases} \tag{18}$$

In Equation (18), Matrix B, Matrix C and Matrix A are, respectively, as follows:

$$B = \begin{bmatrix} 0 & 0 & 0 & 0 & -\frac{P_i}{m_2 L} & 0 & 0 \end{bmatrix}^T$$

$$C = \begin{bmatrix} -1 & 0 & 1 & 0 & 0 & 0 & 0 \\ 0 & 0 & 0 & 0 & 1 & 0 & 0 \end{bmatrix}$$

$$A = \begin{bmatrix} 0 & 1 & 0 & 0 & 0 & 0 & 0 \\ -\frac{k}{m_1} & -\frac{c}{m_1} & -\frac{k_2}{m_1} & -\frac{c_2}{m_1} & -\frac{m_2}{m_1} & \frac{k_2}{m_1} & \frac{c_2}{m_1} \\ 0 & 0 & 0 & 1 & 0 & 0 & 0 \\ 0 & 0 & 0 & 0 & 1 & 0 & 0 \\ -\frac{RP_s}{m_2 L} & 0 & T_1 & T_2 & -T_3 & T_4 & T_5 \\ 0 & 0 & 0 & 0 & 0 & 0 & 1 \\ 0 & 0 & \frac{k_2}{m_3} & \frac{c_2}{m_3} & 0 & -\frac{k_2}{m_3} & -\frac{c_2}{m_3} \end{bmatrix}$$

The parameters T_1 to T_5 in matrix A are as follows:

$$T_1 = \frac{(RP_s - Rk_2)(m_2 m_3) + k_2 c_2 m_2 L}{m_2^2 m_3 L}$$

$$T_2 = \frac{c_2^2 m_2 L - (Rc_2 + k_2 L) m_2 m_3}{m_2^2 m_3 L}$$

$$T_3 = \frac{m_2 R + c_2 L}{m_2 L}$$

$$T_4 = \frac{Rk_2 m_2 m_3 - k_2 c_2 m_2 L}{m_2^2 m_3 L}$$

$$T_5 = \frac{(Rc_2 + k_2 L) m_2 m_3 - c_2^2 m_2 L}{m_2^2 m_3 L}$$

2.2. Robust Controller Design Based on LMI

The maglev system (18) is unable to maintain stable suspension in an open-loop configuration. Consequently, closed-loop control of the system is essential. In practical applications, parameter variations are inevitable. To enhance the robustness of the magnetic levitation system, it is crucial to account for parameter uncertainties during the initial stages of controller design. Fortunately, this challenge can be addressed by transforming the problem into a constrained linear matrix inequality optimization issue. The magnetic levitation system is subsequently modeled as a linear uncertain system and characterized by its state-space representation [43].

$$\begin{cases} \dot{x}(t) = (A + \Delta A)x(t) + (B + \Delta B)u(t) \\ y(t) = Cx(t) \\ x(0) = x_0 \end{cases} \tag{19}$$

In this system, x_0 denotes the initial state of the system. The matrix functions ΔA and ΔB are employed to characterize the uncertainties within the system model, which are

norm-bounded uncertainty matrices of appropriate dimensions. These matrix functions may be formally described as follows:

$$[\Delta A\ \Delta B] = HF(t)[E1\ E2] \tag{20}$$

In this context, the matrices H, E_1, and E_2 are defined as real constant matrices with appropriate dimensions and satisfy the inequality $F^T(t)F(t) \leq I$, where I denotes the identity matrix of the corresponding dimension. For system (20), we introduce a quadratic performance index, which can be formally expressed as follows:

$$J = \int_0^\infty [x^T(t)Qx(t) + u^T(t)R_u u(t)dt \tag{21}$$

In this system, Q denotes the prescribed semidefinite symmetric matrix that encapsulates the weights of the state variables as defined in Equation (18). R_u represents the weight matrix associated with the input and is specified as a symmetric positive definite matrix. The symbol $u(t)$ signifies the control input. Based on these parameters, the definitions are formalized as follows:

Definition 1 ([44]). *For the uncertain system (19) and performance index (21), if there is a control law u(t) and a positive number J*, they can make the closed-loop system asymptotically stable for all allowable uncertainties. Meanwhile, the performance index of closed loop system satisfies $J \leq J^*$, then J* is called a performance upper bound of the uncertainty system (19) and u(t) is a guaranteed performance control law for the uncertain system (19).*

Definition 2 ([44]). *For the uncertain system (19), if there is a linear state feedback control law $u(t) = Kx(t)$, scalar and symmetric positive definite matrix P, they can meet the Lyapunov function $V(x(t),t) = x^TPx$, and the Lyapunov function meets the following inequality (22) for all the $(x(t),t) \in R^n \times R$, $t > 0$ and any initial condition $x(t) = \varphi(t)$. Then the control law $u(t) = Kx(t)$ is the robust quadratic stabilization cost control law.*

$$\dot{V}(x(t),t) \leq -\varepsilon\|x(t)\|^2 \tag{22}$$

In literature [45,46], a robust controller is designed for an automotive suspension system where cross terms are present in the quadratic performance index. Since the quadratic performance index of the maglev system does not include cross terms, this chapter will develop a robust controller by integrating Definitions 1 and 2 and employing the proof methods from references [43,44], etc., to appropriately transform the controller solution method presented in references [45,46]. For detailed proof ideas, please refer to paper [45,46], etc.

Theorem 1. *For the uncertain system (19) and the quadratic performance index (21), if there are positive definite matrix $X, Z \in R^{n\times n}$, matrix $Y \in R^{m\times n}$ and scalar $\eta > 0$, they satisfy the following inequality matrix (23) to all the allowable uncertainties F(t). Then the control law $u(t) = Kx(t)$ is a guaranteed cost control law, V(x(0),0) is a guaranteed cost and the feedback control gain matrix is $K = YX^{-1}$.*

$$\begin{aligned} &\min_{\eta,Y,X,M,Z} Trace(M) \\ \text{s.t.(i)} &\begin{bmatrix} S & (E_1X+E_2Y)^T & X & Y^T \\ * & -\eta & 0 & 0 \\ * & * & -Q^{-1} & 0 \\ * & * & 0 & -R^{-1} \end{bmatrix} < 0 \\ \text{(ii)} &\begin{bmatrix} -M & x^T(0) \\ x(0) & -X \end{bmatrix} < 0 \end{aligned} \tag{23}$$

Here, $S = XA^T + BY + (AX + BY)^T + Z + \eta HH^T$, $KX = Y$, $P^{-1} = X$, $Z = P^{-1}\varepsilon P^{-1}$, and M is a real matrix with an appropriate dimension. η is optimized simultaneously with the controller gain matrix K and the Lyapunov matrix P by the LMI solver to minimize the prescribed performance index while satisfying the robust stability constraints.

By applying Theorem 1, the state feedback gain matrix K for the magnetic suspension system is derived through the linear matrix inequality (LMI) approach.

Controller 1: The expression for u_1 is presented in Equation (24):

$$u_1 = K_1X_1 \tag{24}$$

Controller 2: The expression for u1 is presented in Equation (25):

$$u_2 = K_2X_2 \tag{25}$$

K_1 denotes the feedback gain matrix associated with Controller 1, while K_2 denotes the feedback gain matrix associated with Controller 2. Similarly, X_1 and X_2 represent the feedback state matrices for controllers 1 and 2, respectively. The values are set as $X_1 = [x_2, \dot{x}_2, \ddot{x}_2]$ and $X_2 = [x_1, \dot{x}_1, x_2, \dot{x}_2, \ddot{x}_2, x_3, \dot{x}_3]$. Note: The reason why both Controller 1 and Controller 2 select the vibration acceleration of the levitation electromagnet as the feedback state variable is: The inclusion of acceleration as a state feedback variable is physically motivated by the need to suppress coupling vibrations in the flexible track beam. Unlike position or velocity, acceleration is directly proportional to the inertial forces driving the structural resonance. Feeding back acceleration provides the controller with direct observability of the high-frequency flexible modes, enabling the synthesis of active damping that compensates for the track beam's low inherent damping ratio. This is essential for stabilizing the system on low-stiffness beams where traditional position-velocity feedback fails to prevent resonance divergence.

3. Dynamic Simulation Analysis

Building on Reference [42], this paper optimizes the matrix Q. Specifically, Q is set to [0.13, 0.14, 0.16, 0.04, 0.14, 0.20, 0.20] for Controller 1 and [0.16, 0.04, 0.14] for Controller 2, while R_u remains [0.05] for both.

The related parameters of the coupling maglev system are shown in Table 1 below. Unless otherwise specified in the paper, the mid-span position of the track beam shall be selected as the static suspension point.

Substituting the system parameters from Table 1 into the system matrix A, eigenstructure analysis of the open-loop matrix explicitly reveals a positive real eigenvalue 23. This confirms that the system is inherently unstable without control, thereby necessitating the adoption of a closed-loop control strategy.

Table 1. System parameters.

Symbol	Quantity	Value
m_1	Track beam mass	2400 kg
m_2	Electromagnet mass	375 kg
m_3	Vehicle body mass	500 kg
A_m	Electromagnetic pole area	0.021 m^2
R	Resistance	1 Ω
c_1	Track beam damping	500 N/(m/s)
n	Coil turns	365

3.1. Characteristic Analysis of the Closed Loop System

We assume that the maglev system operates under nominal conditions, implying no parameter perturbations. The maximum dynamic response characteristics of the real part of the characteristic root of the closed-loop system matrix, as the rigidity of the track beam varies from 500 kN/m to 100,000 kN/m, when utilizing Controller 1 and Controller 2, are illustrated in Figure 1 below.

As illustrated in Figure 2, when the rigidity of the track beam increases from 500 kN/m to 100,000 kN/m (the range (500–100,000 kN/m) was selected to cover extreme scenarios: from very flexible elevated guideways (low end) to stiff concrete tracks (high end)), the maximum real part of the characteristic root of the closed-loop system matrix remains negative with Controller 1. In contrast, for Controller 2, this value is only negative when the rigidity exceeds at least 5000 kN/m. This indicates that stable suspension of the maglev system cannot be achieved by Controller 2 when the track beam rigidity is below 5000 kN/m, whereas Controller 1 ensures stable suspension under the low track beam stiffness. Further analysis reveals that when the track stiffness is sufficiently high (e.g., 60,000 kN/m), both state feedback controllers yield nearly identical maximum real parts of the characteristic roots of the closed-loop system matrix. It can thus be inferred that elastic deformation of the track beam is a significant factor influencing the coupling vibration between the track beam and the maglev system. When the rigidity of the track beam is sufficiently high, the vibration of the track beam becomes almost negligible. Consequently, engineering practice suppresses vehicle–track coupling vibration by increasing track beam damping and stiffness.

3.2. Analysis of the Impact of Parameter Perturbations on the Suspension Characteristics of the System

In this section, we investigate the dynamic response characteristics of the maglev system under closed-loop control using Controller 1 when parameter perturbations occur on an elastic track beam with low stiffness, employing the LMI solution method. The rigidity of the track beam is set to 2000 kN/m, and a 20% perturbation in the suspension electromagnet's inductance is assumed (The effect of parameter perturbation on the dynamic characteristics of the maglev system can be equated to the perturbation of parameters such as suspension inductance). If the nominal value of the suspension inductance is denoted as L, it can be observed that when there is a certain degree of perturbation in the suspension inductance, the actual parameter becomes [47]:

$$\frac{1}{\widetilde{L}} = \frac{1}{L}(1 + r_{ng}\delta), |\delta \leq 1| \tag{26}$$

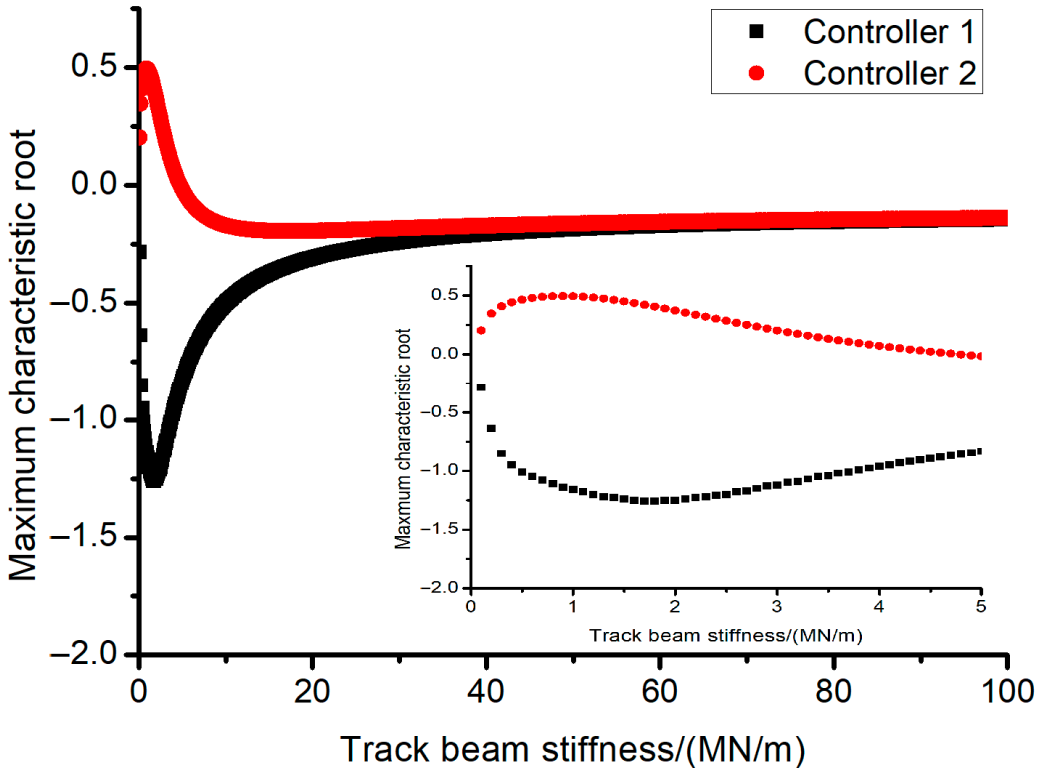


Figure 2. Dynamic characteristic of the maximum characteristic root.

In Equation (26), r_{ng} represents the upper bound of the perturbation range for the inductance parameter. Here, δ is a random variable with a dynamic range of [−1, +1]. Regarding Equation (19), the following ΔA and ΔB can be observed:

$$\Delta A = \begin{bmatrix} 0 & 0 & 0 & 0 & 0 & 0 & 0 \\ 0 & 0 & 0 & 0 & 0 & 0 & 0 \\ 0 & 0 & 0 & 0 & 0 & 0 & 0 \\ 0 & 0 & 0 & 0 & 0 & 0 & 0 \\ -\frac{RP_s \cdot r_{ng}\delta}{m_2 L} & 0 & \frac{R(P_s-k_2)\cdot r_{ng}\delta}{m_2 L} & -\frac{Rc_2 \cdot r_{ng}\delta}{m_2 L} & -\frac{R\cdot r_{ng}\delta}{L} & \frac{Rk_2 \cdot r_{ng}\delta}{m_2 L} & \frac{Rc_2 \cdot r_{ng}\delta}{m_2 L} \\ 0 & 0 & 0 & 0 & 0 & 0 & 0 \\ 0 & 0 & 0 & 0 & 0 & 0 & 0 \end{bmatrix}$$

$$\Delta B = \begin{bmatrix} 0 & 0 & 0 & 0 & -\frac{P_i \cdot r_{ng}\delta}{m_2 L} & 0 & 0 \end{bmatrix}^T$$

When the random number generator (r_{ng}) is set to 1 and the value of δ is 0.2, we can derive from Equation (20) that:

$$\begin{cases} H = \begin{bmatrix} 0 & 0 & 0 & 0 & 0.2/(m_2 L) & 0 & 0 \end{bmatrix}^T \\ E_1 = \begin{bmatrix} -RP_s & 0 & R(P_s - k_2) & -Rc_2 & -m_2 R & Rk_2 & Rc_2 \end{bmatrix} \\ E_2 = [-P_i] \end{cases} \quad (27)$$

In accordance with Theorem 1, the pertinent parameters are introduced and solved utilizing the mincx command of the LMI toolbox. The feedback gain matrix K_{11} and K_{12} for Controller 1 can be derived under conditions of both 20% perturbation and non-perturbation of the suspension inductance in the maglev system, as presented in Equation (28) and Equation (29), respectively. Note: The LMI optimization successfully achieved a feasible solution meeting the required tolerances (1×10^{-3} relative, 1×10^{-6}

absolute); Convergence was exceptional, with the objective minimized to 6.19×10^{-19}, far below the tolerance; The feasibility margin remained substantial, as indicated 14.06% and 0.001%,respectively, constraint saturation within a large feasibility radius ($R = 1.00 \times 10^{9}$); The solvers employed were both from LMI-Lab, which serves as the built-in solver; the former required 98 iterations, while the latter required 43.

$$K_{11} = \begin{bmatrix} -10143 & -418 & 25024 & 1091 & 28 & -548 & -56 \end{bmatrix} \quad (28)$$

$$K_{12} = \begin{bmatrix} -4896 & -200 & 11809 & 511 & 13 & -245 & -25 \end{bmatrix} \quad (29)$$

Under the control of suspension Controller 1, assuming that the suspended electromagnet deviates from the equilibrium position by 2 mm, the suspension gap, vertical displacement of track beam, vertical vibration acceleration of track beam, vertical displacement of suspended electromagnet and vertical vibration acceleration of car body are shown in Figure 3, Figure 4, Figure 5, Figure 6 and Figure 7, respectively.

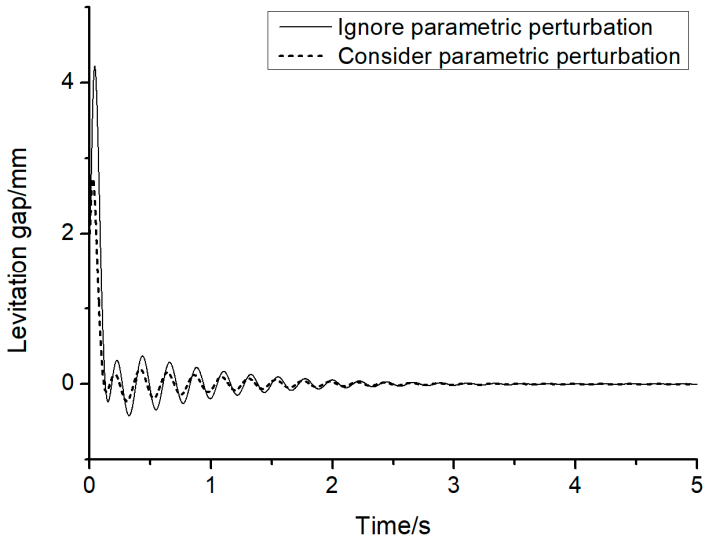


Figure 3. Dynamic response characteristics of levitation gap with Controller 1.

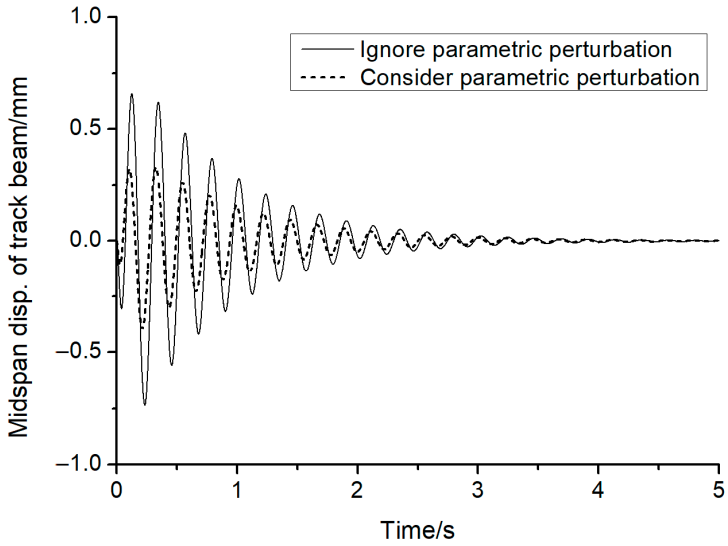


Figure 4. Dynamic response characteristics of track beam displacement with Controller 1.

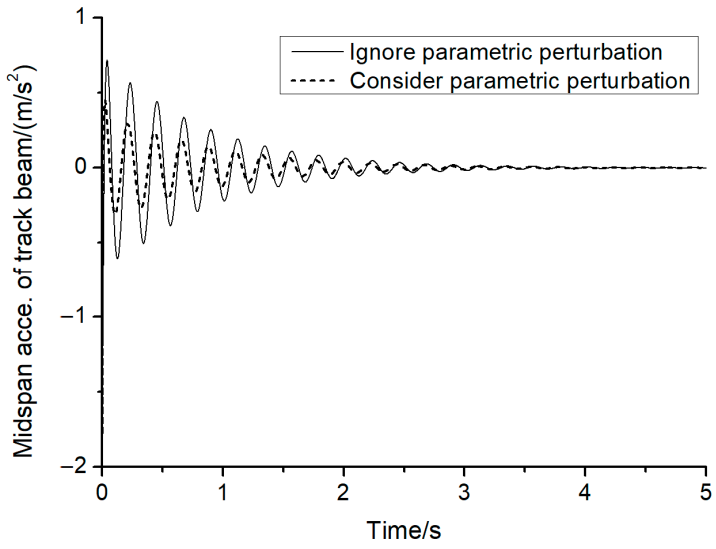


Figure 5. Dynamic response characteristics of track beam acceleration.

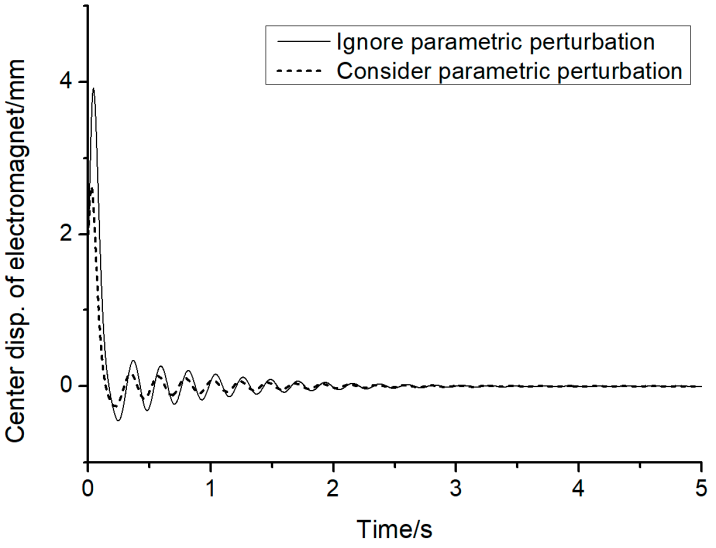


Figure 6. Dynamic response characteristics of electromagnet displacement with Controller 1.

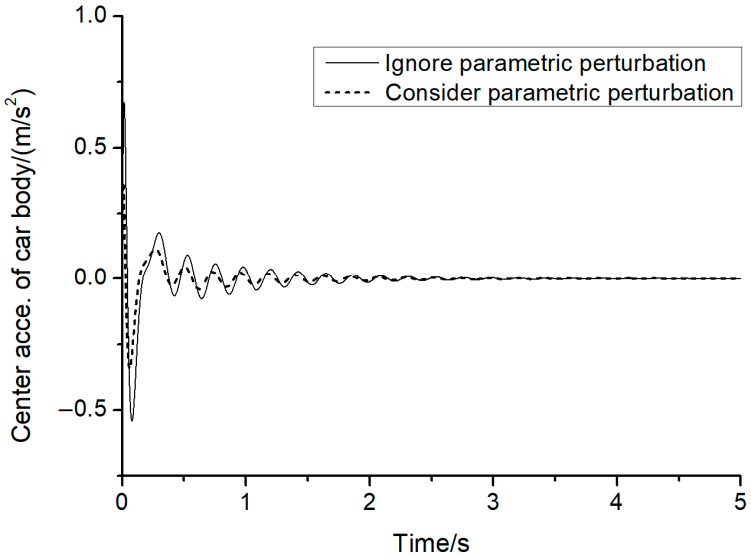


Figure 7. Dynamic response characteristics of car body acceleration.

Based on the analysis from Figures 3–7, when parameter perturbations are present in the maglev system, the maximum fluctuation of the vehicle body's vertical vibration acceleration is approximately 0.7 m/s^2, Root mean square acceleration is 0.09 m/s^2 (Based on the criteria defined in ISO 2631-1, the ride quality is classified as not uncomfortable)and the maximum displacement fluctuation of the track beam is approximately 0.75 mm under the control of a suspension controller designed without considering parameter perturbation. In contrast, when using a suspension controller that accounts for parameter perturbation, the maximum fluctuation of the vehicle body's vertical vibration acceleration is reduced to approximately 0.3 m/s^2, Root mean square acceleration is 0.07 m/s^2 (Based on the criteria defined in ISO 2631-1, the ride quality is classified as not uncomfortable)and the maximum track beam displacement fluctuation is reduced to approximately 0.3 mm. These results indicate that controllers accounting for parameter perturbations significantly outperform those that do not. For instance, the maximum mid-span displacement of the track beam is reduced by 0.45 mm.

Building on the research methodology of References [46,47], specifically from the perspective of the work done by the levitation system on the track beam, this paper employs Controller 1 to investigate the effects of feedback control strategies—considering versus ignoring parameter perturbations—on the coupled vehicle-guideway vibration response characteristics. According to measurements from the Tangshan maglev line, the vibration characteristics of the track beam can be represented by a sine or cosine function of a specific frequency [47]. Since power reflects the rate of energy transfer and is expressed as the product of force and velocity, we propose using the track beam's velocity as input and the suspension force acting on the track beam as output to investigate the impact of varying vibration frequencies. The transfer function can be formulated as follows: $H_{FV}(s) = F(s)/V(s)$. Base on [47], at a given time, with a vibration frequency ω, an amplitude of 0.1 m/s, and employing a sinusoidal function without phase difference to simulate the vibration characteristics of the track beam, i.e., $v(t) = 0.1\sin(wt)$, the electromagnetic force between the track beam and the suspension system can be described by Equation (30):

$$F(t) = 0.1|H_{FV}(jw)|\sin[wt + \angle H_{FV}(jw)] \tag{30}$$

Further analysis reveals that the power exerted by the electromagnetic suspension force on the elastic track beam over a specified time interval is expressed in Equation (31) below:

$$P(w) = \frac{1}{T}\int_0^T F(\psi)V(\psi)d\psi = 0.005\mathrm{Re}[H_{FV}(jw)] \tag{31}$$

By substituting the relevant parameters into Equations (30) and (31), when Controller 1 is utilized, the average power exerted by the suspension system on the track beam, considering both relevant and ignored parametric perturbations under parametric uncertainties, is illustrated in Figure 8 below.

Based on the analysis presented in Figure 8, when the system is subjected to parameter perturbation, disregarding the perturbation in the controller design will result in the track beam transmitting increased vibration energy to the suspension system across most frequency bands. This, in turn, will exacerbate the overall system vibration. Therefore, Figure 8 also elucidates the rationale behind the improved dynamic characteristics of the system when the impact of parameter perturbation is accounted for in the controller design. Based on a more detailed analysis of Figures 1 and 7, it is evident that the system can achieve stable suspension on the flexible track beam by employing a feedback controller that considers the vibration states of the track beam, the suspended electromagnet, and the car body. This stability is achieved because the suspension system effectively absorbs the

vibration energy generated by the track beam across its entire frequency spectrum, thereby ensuring the system remains stably suspended.

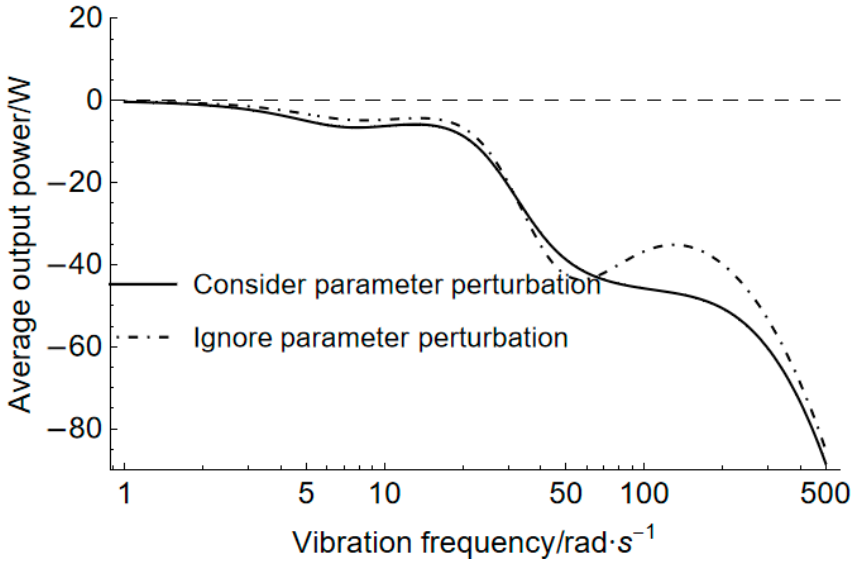


Figure 8. Average Output Power: Analysis with and without Parametric Perturbations.

3.3. Analysis of the Robustness and Track Beam Following Characteristic of Controller 1

In this section, we analyze the robustness of the LMI-based suspension controller under perturbed system parameter. Assuming that the maglev system has reached a stable state, two working conditions are considered. Condition 1: A sinusoidal excitation with an amplitude of 10 mm and a vibration frequency of 5 rad/s is applied vertically to the car body. Condition 2: The suspended electromagnet experiences a pulse excitation with an amplitude of 3 mm and a duration of approximately 0.1 s at 2 s and 6 s, respectively. With the track beam stiffness set at 2000 kN/m, the relevant parameters from Table 1 are utilized. When the inductance of the suspension electromagnet is perturbed by 20%, Controller 1 is employed to perform closed-loop control on the maglev system. Figures 9 and 10 illustrate the dynamic response characteristics of the suspension gap under these two excitation conditions.

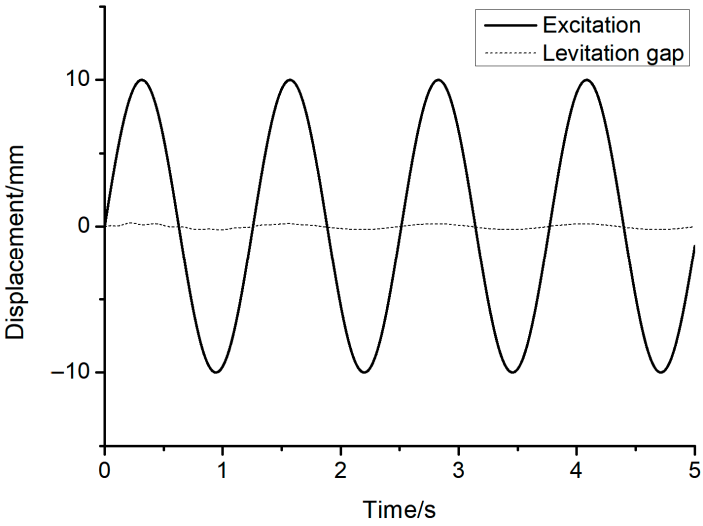


Figure 9. Characteristics of sinusoidal excitation response in suspension gap.

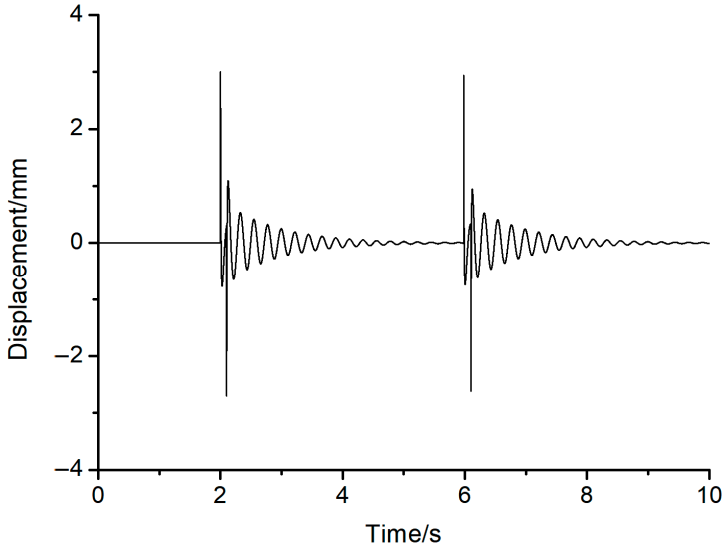


Figure 10. Characteristics of pulse excitation response in suspension gap.

As illustrated in Figure 9, when the vehicle body is subjected to a certain level of external excitation, the dynamic response characteristics of the suspension gap remain virtually unchanged. Figure 10 clearly demonstrates that, upon exposure to a specific degree of pulse excitation, the maglev system can rapidly achieve stable levitation without experiencing significant vehicle-guideway coupling vibration. This indicates that the suspension Controller 1, designed using the LMI solution method, exhibits significant robustness.

To investigate the high-frequency suppression and low-frequency following characteristics of Controller 1 on an elastic track beam, a sinusoidal function with a specified frequency and zero phase difference is applied to the track beam to simulate irregularity excitation. The amplitude of this sinusoidal function is set at 1 mm, with a vibration frequency of 10 rad/s for low-frequency excitation and 120 rad/s for high-frequency excitation. Assuming the track beam stiffness is 2000 kN/m and incorporating the relevant parameters from Table 1, Controller 1 can be utilized to perform closed-loop control on the maglev system. The low-frequency following and high-frequency suppression characteristics of the suspension system are illustrated in Figure 11 and Figure 12, respectively.

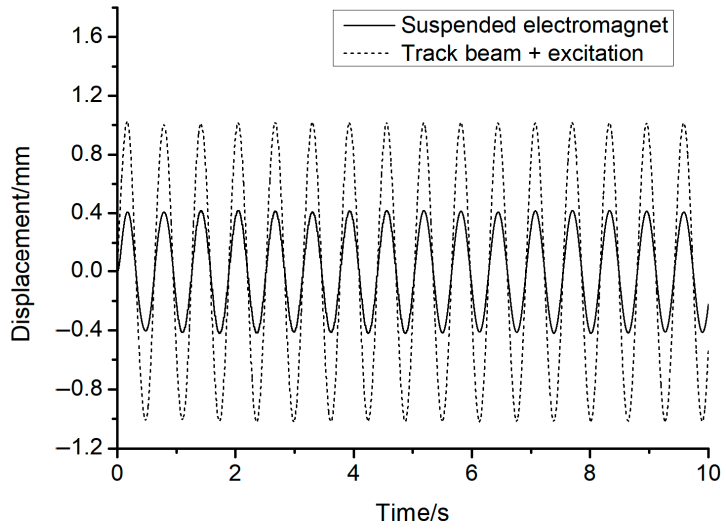


Figure 11. Low-frequency following characteristics of the suspension controller.

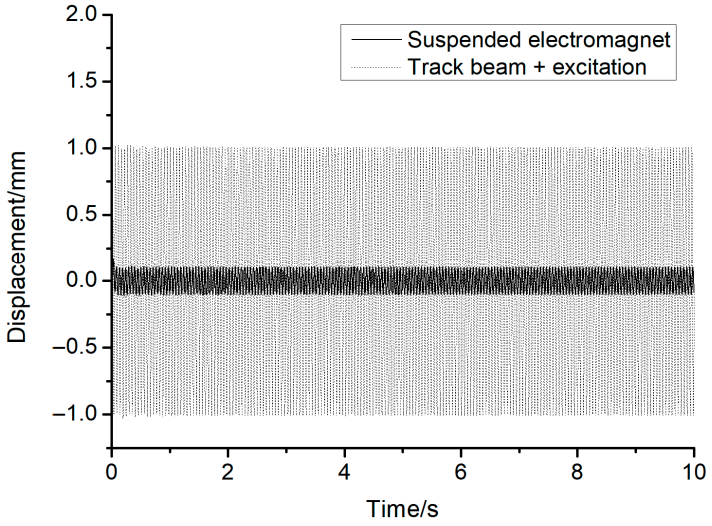


Figure 12. High-frequency suppression characteristics of the suspension controller.

It is evident from the analysis presented in Figure 11 that when the track beam is subjected to low-frequency excitation at a specific frequency and Controller 1 is employed for closed-loop control of the maglev system, the suspended electromagnet demonstrates superior tracking performance in response to the displacement changes and irregularity excitations of the track beam. This indicates that suspension Controller 1 can maintain favorable low-frequency following characteristics even on an elastic track beam with low stiffness, when the system is subject to parameter perturbation.

As illustrated in Figure 12, when the track beam is subjected to high-frequency excitation at a specific frequency and Controller 1 is employed for closed-loop control of the maglev system, the suspended electromagnet exhibits minimal sensitivity to the displacement changes of the track beam and the irregular excitation. Despite the maximum peak value of dynamic displacement change in the track beam and the suspended electromagnet being approximately 1 mm, the maximum peak value of the dynamic displacement change in the suspended electromagnet alone is about only 0.05 mm. This indicates that the suspended electromagnet almost perfectly tracks the absolute reference plane of the track beam. In conclusion, when the system is subject to parameter perturbation, it can be inferred that Controller 1 demonstrates effective high-frequency suppression characteristics on the low-stiffness elastic track beam.

3.4. Optimization of Feedback Parameters for Suspension Controller

An increased number of feedback parameters allows for more precise configuration of the pole positions in the closed-loop system, thereby optimizing dynamic response characteristics such as overshoot and settling time. For instance, in high-dimensional systems, multiple parameters can be adjusted to assign poles to more complex yet desirable regions, simultaneously enhancing the system's interference suppression and robustness. However, this approach may introduce challenges such as elevated computational and implementation complexity, as well as an increased risk of overfitting. Consequently, this section will investigate strategies for employing appropriate state parameter feedback to achieve stable suspension of the system on a flexible track beam. The feedback parameters of Controller 1 are adopted for Controller 3, with the exception of the vibration velocities of the track beam and the vehicle body, which can be expressed as K_{13} based on Equation (28).

$$K_{13} = [-10143 \quad 25024 \quad 1091 \quad 28 \quad -548] \tag{32}$$

Under the control of Controller 1 and Controller 3, the suspension system exerts force on the track beam, as illustrated in Figure 13 below.

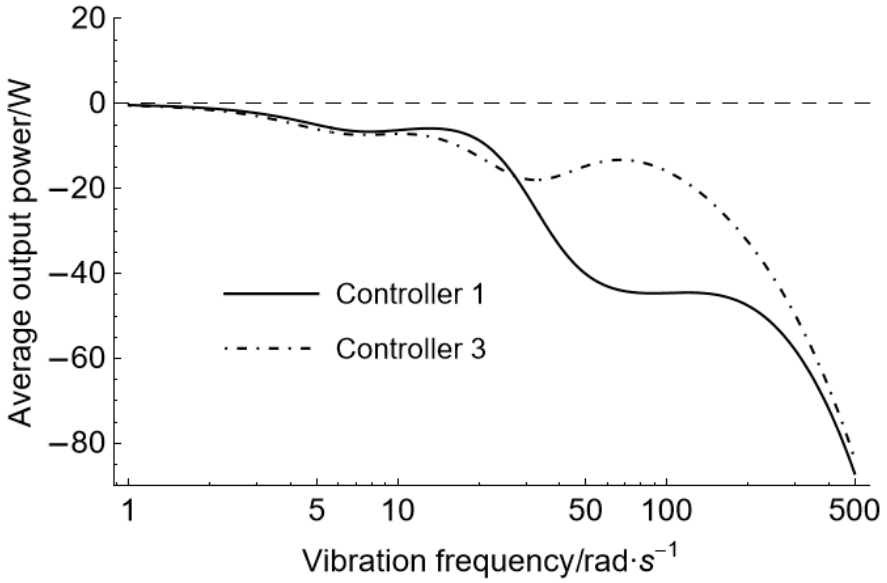


Figure 13. Average output power-different feedback state variables.

Analysis of Figure 13 clearly reveals that Controller 3 exhibits superior vibration energy absorption capabilities in the low-frequency range. Conversely, Controller 1 demonstrates higher efficiency in absorbing vibration energy in the high-frequency range. Based on these observations, we conducted a quantitative analysis of the suspension gap, track beam vibration displacement, and suspended electromagnet vibration displacement at vibration frequencies of approximately 10 rad/s and 30 rad/s, respectively. The results are illustrated in Figures 14–19 (assuming a 2 mm deviation of the suspended electromagnet from its equilibrium position).

Based on the analysis presented in Figures 14–16, Controller 3 effectively achieves stable levitation of the suspension system on the flexible beam. Specifically, the maximum suspension gap is limited to 0.5 mm, and the maximum mid-span displacement of the track beam is approximately 0.6 mm. Further investigation reveals that, generally speaking, when the vibration frequency of the track beam is 10 rad/s, Controller 3 exhibits superior dynamic performance compared to Controller 1.

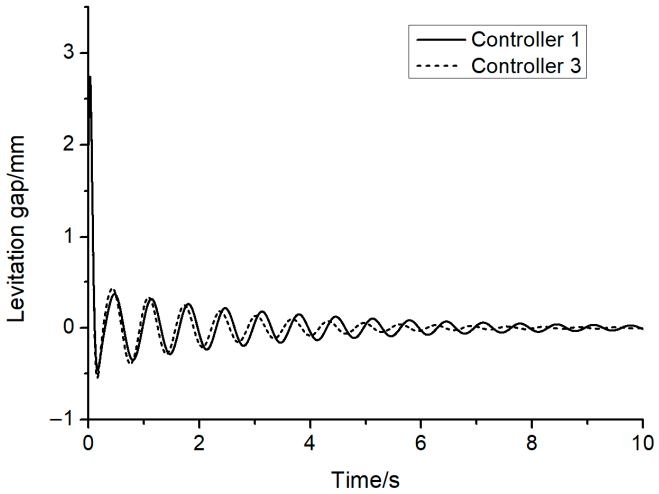


Figure 14. Dynamic response characteristics of levitation gap with Controller 1 and 3.

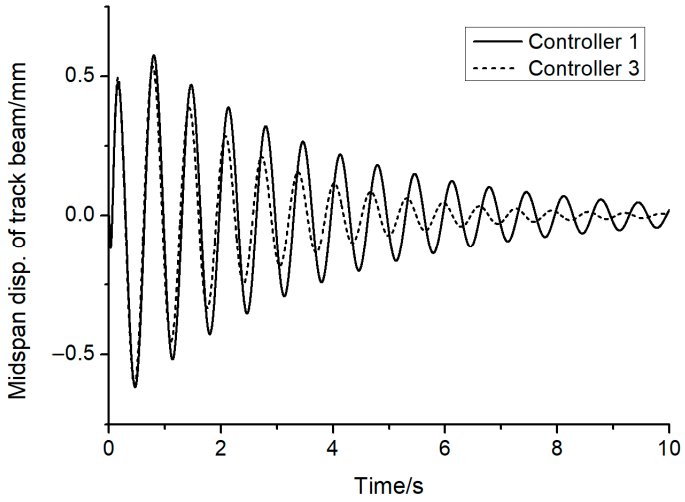


Figure 15. Dynamic response characteristics of track beam displacement with Controller 1 and 3.

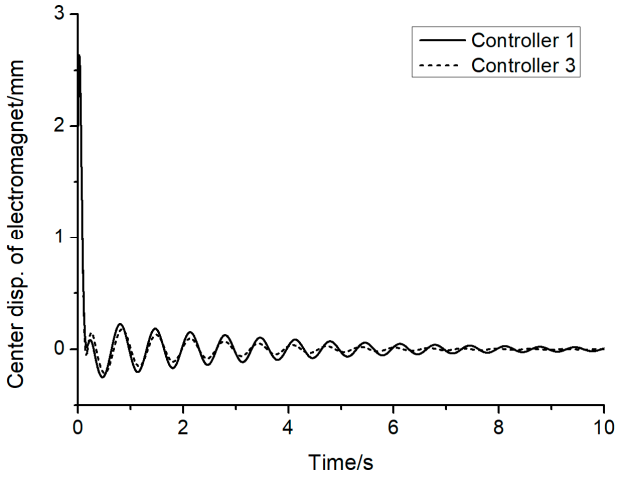


Figure 16. Dynamic response characteristics of electromagnet displacement with Controller 1 and 3.

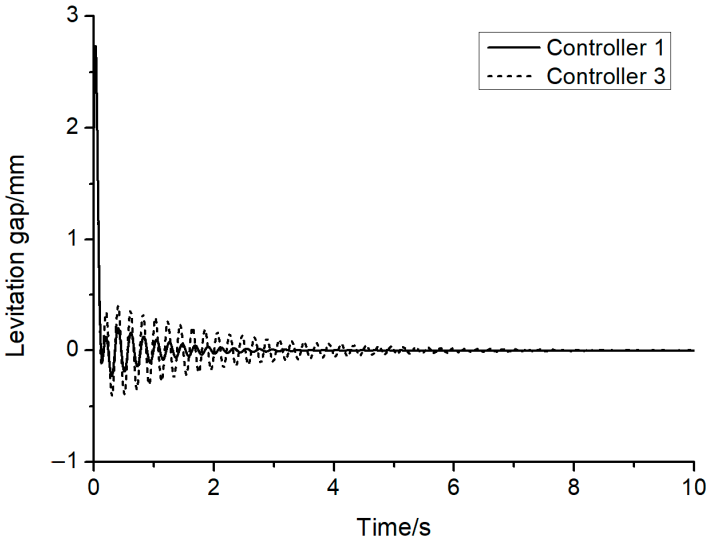


Figure 17. Dynamic response characteristics of levitation gap with Controller 1 and 3.

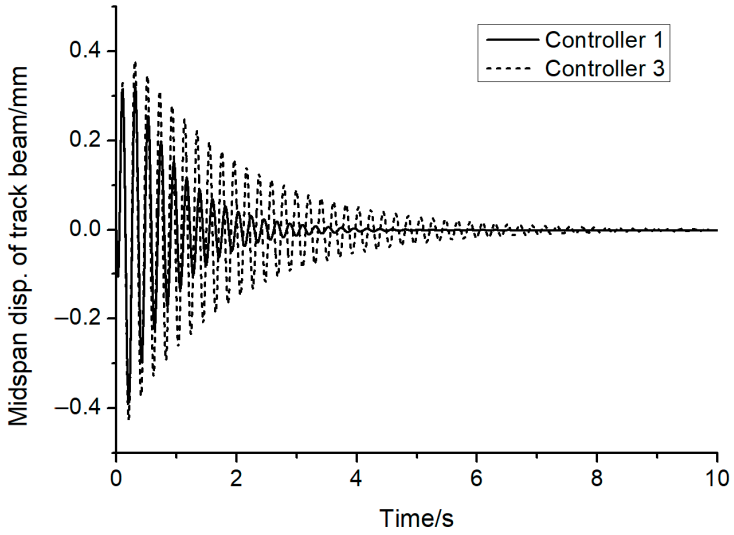


Figure 18. Dynamic response characteristics of track beam displacement with Controller 1 and 3.

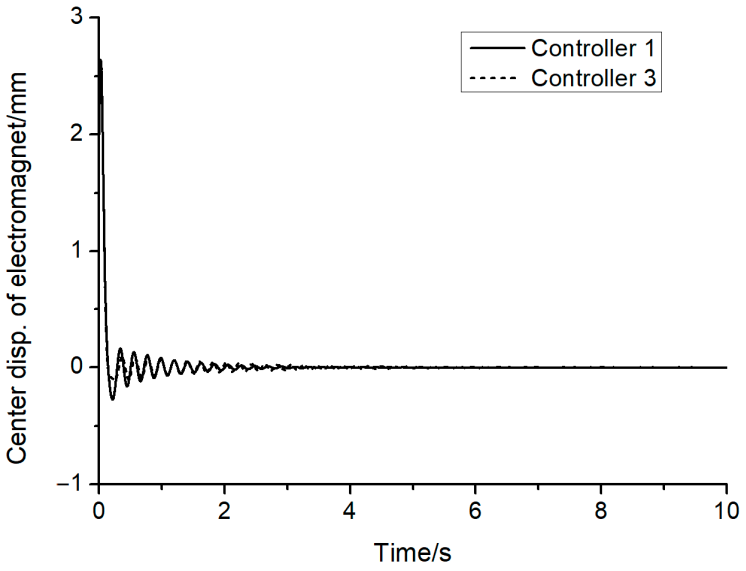


Figure 19. Dynamic response characteristics of electromagnet displacement with Controller 1 and 3.

Further analysis from Figure 14 (Levitation Gap) reveals that both controllers exhibit a similar initial peak deviation. However, the oscillations for Controller 3 decay much more rapidly than those for Controller 1. By approximately t = 6 s, the response of Controller 3 has almost completely settled, while Controller 1 continues to show noticeable, albeit small, oscillations.

Further analysis from Figure 15 reveals that (Track Beam Displacement) the amplitude of oscillation for Controller 3 decreases significantly faster than for Controller 1. At t = 4 s, the oscillations for Controller 3 are already very small, whereas Controller 1's response maintains a significantly higher amplitude. This indicates that Controller 3 damps the vibrations of the flexible track beam much more effectively in this scenario.

To sum up, Controller 3 demonstrates a significantly shorter settling time than Controller 1. It brings both the levitation gap and the track beam displacement to a steady state much faster.

Based on the analysis presented in Figures 17–19, Controller 1 effectively achieves stable levitation of the suspension system on the flexible beam. Specifically, the maximum suspension gap is limited to 0.2 mm, and the maximum mid-span displacement of the track beam is approximately 0.4 mm. Further investigation reveals that, generally speaking,

when the vibration frequency of the track beam is 30 rad/s, Controller 1 exhibits superior dynamic performance compared to Controller 3.

Further analysis from Figure 16 (Levitation Gap) reveals that both controllers exhibit a similar initial peak deviation. However, the oscillations for Controller 1 decay significantly faster than those for Controller 3. By $t \approx 1.7$ s, the response of Controller 1 has almost completely settled. In contrast, Controller 3's response continues to oscillate with noticeable amplitude until after t = 4 s. To sum up, Controller 1 has a much shorter settling time for the levitation gap compared to Controller 3.

Further analysis from Figure 17 reveals that (Track Beam Displacement) both controllers start with a similar peak displacement (~0.3 mm), their damping characteristics are vastly different. The vibrations induced in the flexible track beam are damped out extremely quickly by Controller 1. Its oscillations are nearly gone by t = 2.5 s. Controller 3, however, allows the track beam to vibrate for a much longer duration. Significant oscillations persist beyond t = 6 s. Therefore, Controller 1 demonstrates superior damping performance and a significantly shorter settling time for the track beam displacement compared to Controller 3.

4. Conclusions

This paper proposed a robust state-feedback control strategy for maglev vehicle–track coupling systems, addressing the critical challenges posed by parameter perturbations and flexible track dynamics. By synthesizing the controller via Linear Matrix Inequalities (LMI), we established a rigorous framework that guarantees closed-loop stability while optimizing vibration suppression. The main conclusions are summarized as follows:

1. In the presence of parametric perturbation within the suspension system, Controller 1, which is based on Linear Matrix Inequalities (LMI), can achieve stable system suspension on a flexible beam. Furthermore, the system demonstrated resilience against $\pm 20\%$ variations in electromagnetic inductance. Simultaneously, the system exhibits excellent robustness along with superior high-frequency suppression and low-frequency tracking characteristics. At high-frequency excitations (120 rad/s), the controller successfully decoupled the electromagnet from track vibrations; while track beam displacement reached 1.0 mm, the resulting electromagnet fluctuation was limited to merely 0.05 mm.
2. If the system experiences parameter perturbation, taking into account its impact on the suspension system, the controller designed with this consideration exhibits superior dynamic characteristics compared to one designed without acknowledging such influence. Such as, peak car body acceleration was reduced from approximately 0.7 m/s^2 to 0.3 m/s^2 and peak car body displacement was reduced from approximately 0.75 mm to 0.3 mm
3. To enhance the dynamic characteristics of the system on the flexible track beam, various state feedback variables can be selectively applied based on distinct vibration frequency ranges. Such as when the vibration frequency of the track beam is 30 rad/s, Controller 1 exhibits superior dynamic characteristics compared to Controller 3; when the vibration frequency of the track beam is 10 rad/s, Controller 3 exhibits superior dynamic performance compared to Controller 1.

5. Limitations and Future Work

It should be noted that this study models the track beam as a linear elastic structure, excluding strong geometric nonlinearities (e.g., large deformation stiffening) and complex stochastic track imperfections that could shift resonance frequencies in real-world scenarios. Furthermore, several limitations warrant acknowledgment: (1) stability analysis relies solely on eigenvalue real parts, omitting damping ratios and modal insights; (2) the lack of

Monte Carlo simulations and sensitivity analysis limits statistical validation; (3) actuator saturation constraints were ignored, potentially affecting practical applicability; (4) the relationship between parameter sensitivity and robustness was not discussed; (5) the characteristics of Controller 3 are not theoretically justified through modal or frequency response analysis.

Future work will incorporate nonlinear beam theories and stochastic track models to validate performance under extreme conditions, followed by hardware-in-the-loop and experimental verification. Additionally, we plan to develop multi-vehicle simulations to investigate long-term cumulative effects, while expanding robustness analyses to include mass fluctuations, damping errors, and time delays. Finally, we will quantify robustness margins and benchmark the proposed strategy against PID and sliding mode controllers.

Author Contributions: Conceptualization, X.C.; methodology, K.W.; software, K.W. and X.C.; validation, K.W., X.C. and J.H.; formal analysis, K.W.; investigation, W.M.; resources, W.M.; data curation, J.H.; writing—original draft preparation, K.W.; writing—review and editing, J.H.; visualization, J.H.; supervision, W.M.; project administration, W.M.; funding acquisition, J.H. and K.W. All authors have read and agreed to the published version of the manuscript.

Funding: This work was supported by the Science and Technology Program Project of Leshan City (grant number: 25SYYJC0013), Projects approved by Leshan Vocational and Technical College (grant number: KY2025027).

Institutional Review Board Statement: Not applicable.

Informed Consent Statement: Not applicable.

Data Availability Statement: The original contributions presented in this study are included in the article. Further inquiries can be directed to the corresponding author.

Conflicts of Interest: The authors declare no conflicts of interest.

References

1. Suwarno, I.; Maarif, A. Robust Integral State Feedback Using Coefficient Diagram in Magnetic Levitation System. *IEEE Access* **2020**, *8*, 57003–57011. [CrossRef]
2. Lee, H.W.; Kim, C.; Lee, J. Review of maglev train technologies. *IEEE Trans. Magn.* **2006**, *42*, 1917–1925. [CrossRef]
3. Gong, J. Structural form and dynamic characteristics of high-speed maglev separated track beam. *J. Vib. Eng. Technol.* **2022**, *10*, 2283–2291. [CrossRef]
4. Song, Y.; Lin, G.; Ni, F.; Xu, J.; Chen, C. Study on Coupled Vertical Vehicle-Bridge Dynamic Performance of Medium and Low-Speed Maglev Train. *Appl. Sci.* **2021**, *11*, 5898. [CrossRef]
5. Cui, Y.; Guo, X.; Mao, H.; Liu, J. Research on the Dynamic Characteristics of a Typical Medium–Low-Speed Maglev Train–Bridge System Influenced by the Transverse Stiffness of Pier Tops. *Appl. Sci.* **2025**, *15*, 6628. [CrossRef]
6. Kim, K.J.; Jong, B.H.; Han, H.S. Coupled vibration analysis of maglev vehicle-guideway while standing still or moving at low speeds. *Veh. Syst. Dyn.* **2015**, *53*, 587–601. [CrossRef]
7. Zhou, D.F.; Hansen, C.H.; Li, J. Review of coupled vibration problems in EMS maglev vehicle. *J. Acoust. Vib.* **2010**, *15*, 10–23. [CrossRef]
8. Lengyel, G.; Kocsis, A. Vehicle-guideway interaction in maglev systems using a continuously coupled, deformable model. *J. Eng. Mech.* **2014**, *140*, 182–192. [CrossRef]
9. Hu, C.Y.; Chen, K.C.; Chen, J.S. Dynamic Interaction of a Distributed Supported Guideway and a Asymmetrical Multimagnet Suspension Vehicle with Unbalanced Mass. *J. Mech.* **2010**, *26*, 1–14. [CrossRef]
10. Li, X.Z.; Wang, D.X.; Geng, J. Study on the influence of F-rail in vertical coupling vibration of low-medium speed maglev train-bridge system. *China Civ. Eng. J.* **2017**, *50*, 97–106.
11. Wang, Z.L.; Xu, Y.L.; Li, G.Q. Modelling and validation of coupled high-speed maglev train-and-viaduct systems considering support flexibility. *Veh. Syst. Dyn.* **2019**, *57*, 161–197. [CrossRef]
12. Han, J.B.; Han, H.S.; Kim, S.S. Design and validation of a slender guideway for maglev vehicle by simulation and experiment. *Veh. Syst. Dyn.* **2016**, *54*, 370–385. [CrossRef]

13. Han, J.B.; Han, H.S.; Li, J.M. Dynamic modeling and simulation of EMS maglev vehicle to evaluate the levitation stability and operational safety over an elastic segmented switch track. *J. Mech. Sci. Technol.* **2018**, *32*, 2987–2998. [CrossRef]
14. Li, J.H.; Li, J.; Zhou, D.F. The active control of maglev stationary self-excited vibration with a virtual energy harvester. *IEEE Trans. Ind. Electron.* **2015**, *62*, 2942–2951. [CrossRef]
15. Li, J.H.; Li, J.; Zhou, D.F. Maglev self-excited vibration suppression with a virtual sky-hooked damper. *J. Cent. South Univ.* **2016**, *23*, 1363–1371. [CrossRef]
16. Wang, L.C.; Li, J.H.; Zhou, D.F. Principle analysis and simulation verification on the vehicle-bridge coupled self-excited vibration of maglevs. *J. Vib. Shock* **2017**, *36*, 14–19.
17. Sun, Y.; Xu, J.; Qiang, H.; Wang, W.; Lin, G. Hopf bifurcation analysis of maglev vehicle–guideway interaction vibration system and stability control based on fuzzy adaptive theory. *Comput. Ind.* **2019**, *108*, 197–209. [CrossRef]
18. Zhang, L.; Huang, L. Hopf Bifurcation Analysis for a Maglev System with Two Time Delays. *Mech. Syst. Signal Process.* **2025**, *224*, 112006. [CrossRef]
19. Feng, Y.; Zhao, C.; Wu, D.; Xie, H.; Tong, L. Effect of levitation gap feedback time delay on the EMS maglev vehicle system dynamic response. *Nonlinear Dyn.* **2023**, *111*, 7137–7156. [CrossRef]
20. Chen, M.; Wu, R.; Chen, L. Spatio temporal patterns induced by Turing and Turing–Hopf bifurcation in a predator–prey system. *Appl. Math. Comput.* **2020**, *380*, 125300.
21. Zhang, Z.; Zhang, L. Hopf bifurcation of time-delayed feedback control for maglev system with flexible guideway. *Appl. Math. Comput.* **2013**, *219*, 6106–6112. [CrossRef]
22. Du, Y.; Niu, B.; Wei, J. Two delays induce Hopf bifurcation and double Hopf bifurcation in a diffusive Leslie–Gower predator–prey system. *Chaos* **2019**, *29*, 013101. [CrossRef]
23. Zhang, M.; Luo, S.H.; Gao, C. Research on the mechanism of a newly developed levitation frame with mid-set air spring. *Veh. Syst. Dyn.* **2018**, *56*, 1797–1816. [CrossRef]
24. Li, M.; Luo, S.H.; Ma, W.H. Experimental and numerical investigations of the dynamic responses of low and medium speed maglev train-track-bridge coupled system. *Veh. Syst. Dyn.* **2022**, *60*, 1555–1578. [CrossRef]
25. Cui, Y.; Shen, G.; Wang, H. Maglev vehicle-guideway coupling vibration test rig based on the similarity theory. *J. Vib. Control* **2016**, *22*, 286–2953. [CrossRef]
26. Li, S.Q.; Zhang, K.L. Research of maglev train dynamics simulation based on levitation control algorithm. *J. Syst. Simul.* **2015**, *27*, 179–184.
27. Zhou, D.F.; Hansen, C.H.; Li, J. Suppression of maglev vehicle-girder self-excited vibration using a virtual tuned mass damper. *J. Sound Vib.* **2011**, *330*, 883–901. [CrossRef]
28. Liu, M.; Fu, S.; Wu, H.; Liang, X.; Zhang, W.; Zeng, X. Predictive control based on LSTM for suspension operation of maglev vehicle. *J. Vib. Control* **2025**, *31*, 2351–2365. [CrossRef]
29. Xu, J.; Sun, Y.; Gao, D. Dynamic modeling and adaptive sliding mode control for a maglev train system based on a magnetic flux observer. *IEEE Access* **2018**, *6*, 31571–31579. [CrossRef]
30. Ni, F.; Zheng, Q.; Xu, J. Nonlinear control of a magnetic levitation system based on coordinate transformations. *IEEE Access* **2019**, *7*, 164444–164452. [CrossRef]
31. Zhang, W.J.; Ling, Z.J.; Zhang, R.Y. Design and applications of the maglev train suspension control algorithm via the improved tracking differentiator. *J. Railw. Sci. Technol.* **2023**, *20*, 3954–3964.
32. Chen, P.; Shi, T.C.; Yu, M.Y. Self-learning model reference adaptive levitation control strategy. *J. Southwest Jiaotong Univ.* **2023**, *58*, 799–807.
33. Long, Z.Q.; Hao, A.M.; Cao, C.K. Sensitivity constrained robust controller design of suspension controller for maglev train. *Control Theory Appl.* **2004**, *21*, 804–808.
34. Sun, Y.G.; Li, W.L.; Lin, G.B. Dynamic modeling and nonlinear control research on magnetic suspension systems of low-speed maglev train. *J. Tongji Univ. Nat. Sci.* **2017**, *45*, 741–749.
35. Hu, K.T.; Xu, J.; Liu, Z.G. Reinforcement learning-based suspension control for electromagnetic suspension maglev trains. *J. Tongji Univ. Nat. Sci.* **2023**, *51*, 332–340.
36. Gao, D.G.; Sun, Y.G.; Luo, S.H. Deep learning controller design of embedded control system for maglev train via deep belief network algorithm. *Des. Autom. Embed. Syst.* **2020**, *24*, 161–181. [CrossRef]
37. Ren, Q.; Zhang, J.M.; Zhou, H.H. Robust adaptive levitation control for medium and low-speed maglev with magnetic saturation and eddy current effect. *J. Vib. Eng. Technol.* **2024**, *12*, 2835–2849. [CrossRef]
38. Tao, X. Research of Key Design Parameters for Low-Speed Magnetic Levitation Rail Beam. Ph.D. Thesis, Tongji University, Shanghai, China, 2008.
39. Wang, H.; Zhong, X.B.; Shen, G. Analysis and experimental study on the maglev vehicle-guideway interaction based on the full-state feedback theory. *J. Vib. Control* **2015**, *21*, 408–416. [CrossRef]
40. Wang, H.; Zhong, X.B.; Shen, G. Control strategy of maglev on elastic track. *J. Traffic Transp. Eng.* **2013**, *13*, 33–38, 46.

41. Liu, H.K.; Hao, A.M.; Chang, W.S. On control methods of the magnetic suspension system on elastic track. *Control Eng. China* **2008**, *15*, 392–394, 415.
42. Wang, K.R.; Luo, S.H.; Chen, X.H. Way of suppressing vehicle-guideway coupling vibration for maglev system based on AHP. *J. China Railw. Soc.* **2020**, *42*, 29–35.
43. Yu, L. *Robust Control—Linear Matrix Inequality Processing Method*; Tsinghua University Press: Beijing, China, 2002.
44. Su, H.Y. *Robust Control Theory for Uncertain Time-Delay Systems*; Science Press: Beijing, China, 2007.
45. Wang, P.; Song, P.Y.; Zhang, J.Y. Robust control for self-powered active suspension with time-delay in actuator. *Control Theory Appl.* **2012**, *29*, 1609–1615.
46. Wang, P. Self-Powered Active Suspension for Railway Vehicles. Ph.D. Thesis, Southwest Jiaotong University, Chengdu, China, 2015.
47. Li, J.H. The Vibration Control Technology of EMS Maglev Vehicle-Bridge Coupled System. Ph.D. Thesis, National University of Defense Technology, Changsha, China, 2015.

Disclaimer/Publisher's Note: The statements, opinions and data contained in all publications are solely those of the individual author(s) and contributor(s) and not of MDPI and/or the editor(s). MDPI and/or the editor(s) disclaim responsibility for any injury to people or property resulting from any ideas, methods, instructions or products referred to in the content.